

# Application of deep learning technique to the sea surface height prediction in the South China Sea

Tao Song<sup>1, 6</sup>, Ningsheng Han<sup>1</sup>, Yuhang Zhu<sup>2, 3, 5</sup>, Zhongwei Li<sup>1</sup>, Yineng Li<sup>2, 3, 4</sup>, Shaotian Li<sup>2, 3</sup>, Shiqiu Peng<sup>2, 3, 4, 5\*</sup>

<sup>1</sup> College of Computer and Communication Engineering, China University of Petroleum (East China), Qingdao 266580, China

<sup>2</sup> State Key Laboratory of Tropical Oceanography, South China Sea Institute of Oceanology, Chinese Academy of Sciences, Guangzhou 510301, China

<sup>3</sup> Southern Marine Science and Engineering Guangdong Laboratory (Guangzhou), Guangzhou 511458, China

<sup>4</sup> Key Laboratory of Science and Technology on Operational Oceanography, Chinese Academy of Sciences, Guangzhou 511458, China

<sup>5</sup> Guangxi Key Laboratory of Marine Disaster in the Beibu Gulf, Bubei Gulf University, Qinzhou 535011, China

<sup>6</sup> Department of Artificial Intelligence, Faculty of Computer Science, Polytechnical University of Madrid, Boadilla del Monte 28660, Madrid, Spain

Received 26 August 2020; accepted 16 September 2020

© Chinese Society for Oceanography and Springer-Verlag GmbH Germany, part of Springer Nature 2021

## Abstract

A deep-learning-based method, called ConvLSTMP3, is developed to predict the sea surface heights (SSHs). ConvLSTMP3 is data-driven by treating the SSH prediction problem as the one of extracting the spatial-temporal features of SSHs, in which the spatial features are “learned” by convolutional operations while the temporal features are tracked by long short term memory (LSTM). Trained by a reanalysis dataset of the South China Sea (SCS), ConvLSTMP3 is applied to the SSH prediction in a region of the SCS east off Vietnam coast featured with eddied and offshore currents in summer. Experimental results show that ConvLSTMP3 achieves a good prediction skill with a mean RMSE of 0.057 m and accuracy of 93.4% averaged over a 15-d prediction period. In particular, ConvLSTMP3 shows a better performance in predicting the temporal evolution of mesoscale eddies in the region than a full-dynamics ocean model. Given the much less computation in the prediction required by ConvLSTMP3, our study suggests that the deep learning technique is very useful and effective in the SSH prediction, and could be an alternative way in the operational prediction for ocean environments in the future.

**Key words:** deep learning, sea surface height prediction, convolutional operation, long short term memory

**Citation:** Song Tao, Han Ningsheng, Zhu Yuhang, Li Zhongwei, Li Yineng, Li Shaotian, Peng Shiqiu. 2021. Application of deep learning technique to the sea surface height prediction in the South China Sea. *Acta Oceanologica Sinica*, 40(7): 68–76, doi: 10.1007/s13131-021-1735-0

## 1 Introduction

Sea surface heights (SSHs) are one of the key factors affecting algae growth, fish distribution and coastal city flooding. It is also vital to marine engineering such as offshore oil production and offshore aquaculture. The change of SSHs is associated with various dynamical processes in the ocean, including mesoscale eddies, waves, currents, tides, etc. As such, the prediction of SSHs has always been a challenge for the oceanographers. Currently, numerical models based on physical equations are usually used to predict SSHs; although the prediction skills are acceptable, considerable uncertainties still exist. On the other hand, the prediction using numerical models requires large computational re-

sources and thus it time consuming, which may not satisfy the need of some emergency situations.

In the last several decades, oceanic data (including *in situ* observations and reanalysis data) are rapidly accumulated, which makes it feasible to use artificial intelligence (AI) for marine environmental prediction. As a boosting technique, it has been found that deep learning can both track spatial features and temporal changing of the marine environment factors from large amount of data through convolutional operations (e.g., convolutional neural network, CNN; Ji et al., 2013; Shin et al., 2016; Zhang et al., 2016; Huang et al., 2017) and recurrent patterns (e.g., recurrent neural network, RNN; Cho et al., 2014), respectively. For

Foundation item: The National Key Research and Development Program under contract Nos 2018YFC1406204 and 2018YFC1406201; the Guangdong Special Support Program under contract No. 2019BT2H594; the Taishan Scholar Foundation under contract No. tsqn201812029; the National Natural Science Foundation of China under contract Nos U1811464, 61572522, 61572523, 61672033, 61672248, 61873280, 41676016 and 41776028; the Natural Science Foundation of Shandong Province under contract Nos ZR2019MF012 and 2019GGX101067; the Fundamental Research Funds of Central Universities under contract Nos 18CX02152A and 19CX05003A-6; the fund of the Shandong Province Innovation Researching Group under contract No. 2019KJN014; the Key Special Project for Introduced Talents Team of the Southern Marine Science and Engineering Guangdong Laboratory (Guangzhou) under contract No. GML2019ZD0303.

\*Corresponding author, E-mail: [speng@scsio.ac.cn](mailto:speng@scsio.ac.cn)

instance, CNN was applied to predict the SST or SSH changes by inputting continuous time series of SST or SSH images (Braakmann-Folgmann et al., 2017; De Bézenac E et al., 2019), while a multi-layer fully connected neural network was used to predict short-term SSHs in the Gulf of Mexico (Zeng et al., 2015). It is also worthwhile to note that Kumar et al. (2017) tried to predict the daily wave heights in different geographical regions using sequential learning algorithms by Minimal Resource Allocation Network, and meanwhile Zhang et al. (2017) used long short term memory (LSTM) (Hochreiter and Schmidhuber, 1997; Ma et al. 2015) to make prediction for sea surface temperatures (SSTs). More recently, Yang et al. (2020) developed mask R-CNN method for water-body segmentation, and Song et al. (2020) proposed a deep-learning-based dual path gated recurrent unit model for sea surface salinity prediction. All these attempts to make prediction of marine environmental variables using AI-based methods achieve encouraging results with acceptable prediction skills.

The combination of convolution operations with LSTM model, called ConvLSTM models, had been proposed and applied to predict continuous radar images (Shi et al., 2015). Similar to SSTs, the changes of SSHs are associated with both temporal evolution and spatial variation; therefore, it is appropriate to employ LSTM to track the SSH temporal evolution as what Zhang et al. (2017) did for SSTs, while the spatial variation features of SSHs among neighboring grids are “learned” by using convolutional operations on SSH values of the grids. As such, a variant of ConvLSTM, named ConvLSTMP3, is proposed in this study, which has multiple parallel sub-network structures similar to those of some previous studies (Szegedy et al., 2015, 2016). In ConvLSTMP3, the convolution operation is embedded inside the LSTM model for tracking changes of spatial information in time series data. Through multiple parallel sub-network structures, the proposed ConvLSTMP3 can fully extract the spatial-temporal features of SSHs in a region and then merge them into a one-dimensional vector. It is worth noting that, the SSH values rather than SSH images are used in training the ConvLSTMP3, which facilitates a more efficient prediction of the SSH values in the coming days.

A region of the South China Sea (SCS), which is located east off Vietnam coast and featured with mesoscale eddies and offshore currents in summer, is chosen for the experiment of SSH

prediction by our ConvLSTMP3 model. Mesoscale eddies refer to cyclonic or anticyclonic vortexes in the ocean with a diameter of 100–300 km and a life span of 2–10 months, which are heavily related with dynamical and biochemical processes and play an important role in the mass and energy transport as well as the chlorophyll and fishery distribution (McWilliams, 1985; Seki et al., 2001; Reckinger et al., 2014; Zhang et al., 2014a) in the ocean. The cyclonic (anticyclonic) mesoscale eddies with cold (warm) cores correspond to low (high) SSHs (Mason et al., 2014; Zhang et al., 2014b). The daily SSHs from the reanalysis dataset of South China Sea (REDOS) (Zeng et al., 2014) from 1 January 1992 to 31 December 2011 with a resolution of  $(1/10)^\circ \times (1/10)^\circ$  are used for the deep learning, which count to a sample number of 7 305 (days) in time. To our best knowledge (Morrow et al., 1994; Soong et al., 1995; Iudicone et al., 1998; Jacobs et al., 1999; Wang et al., 2000; Zeng et al., 2014; Weiss and Grooms, 2017), this is the first attempt of using ConvLSTM model to predict SSHs in mesoscale areas.

The rest of the paper is organized as follows. Section 2 describes different prediction models based on deep learning techniques and the experimental design. Section 3 presents the results. The conclusions are given in the final section.

## 2 Methods

### 2.1 ConvLSTM

Before introducing ConvLSTM (Fig. 1), it is necessary to recall basic notions of LSTM. It is an improved RNN having a number of memory cells  $C_t$  (Eq. (1)), each of which has an input gate  $i_t$  (Eq. (2)), forgetting gate  $f_t$  (Eq. (3)), output gate  $o_t$  (Eq. (4)) and  $h_t$  (Eq. (5)). LSTM can preserve meaningful information and remove useless information through the three gates. The input and output of the memory cells are one-dimensional vectors, and LSTM may have multiple memory units named fully connected LSTM. The key equations of LSTM are shown as follows:

$$C_t = f_t \circ C_{t-1} + i_t \circ \tanh(W_{xc}x_t + W_{hc}h_{t-1} + b_c), \quad (1)$$

$$i_t = \sigma(W_{xi}x_t + W_{hi}h_{t-1} + W_{ci}C_{t-1} + b_i), \quad (2)$$

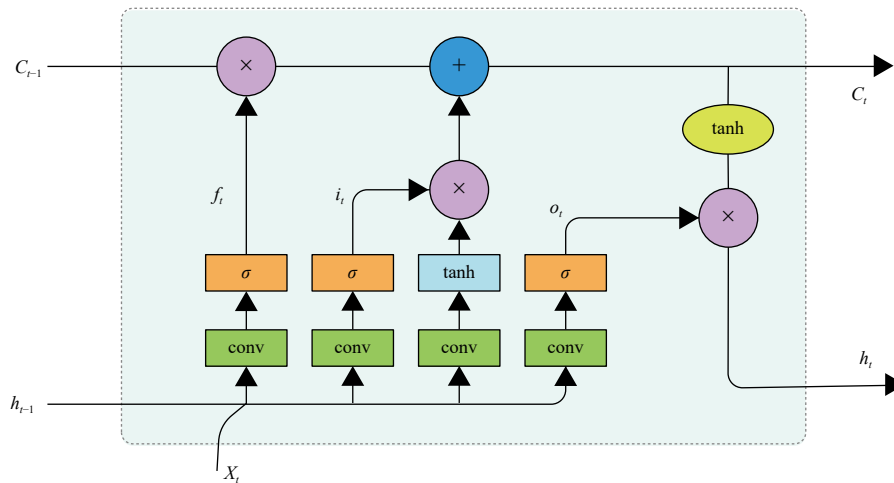


**Fig. 1.** A schematic flow chart of ConvLSTM. “Conv” represents the convolution operation. Spatial information is coded as input in LSTM for tracking temporal evolution. The size of convolutional kernel can be  $3 \times 3$ ,  $5 \times 5$  and  $7 \times 7$ . Multiple kernels are denoted by allows.

$$f_t = \sigma(W_{xf}x_t + W_{hf}h_{t-1} + W_{cf}c_{t-1} + \mathbf{b}_f), \quad (3)$$

$$o_t = \sigma(W_o[h_{t-1}, x_t] + \mathbf{b}_o), \quad (4)$$

$$h_t = o_t \circ \tanh(c_t), \quad (5)$$

where “ $\circ$ ” denotes the Hadamard product,  $W$  and  $\mathbf{b}$  are the weight matrices of the neural network,  $x$  is the input vector, and  $\sigma$  is the sigmoid activation function.

ConvLSTM is a variant of LSTM, which embeds convolution operations inside LSTM cells, and it is designed to deal with the problem of spatial-temporal sequence (Shi et al., 2015). ConvLSTM can extract spatial-temporal information through the convolution multiplication. Since convolution kernel has the feature of weight sharing, ConvLSTM network has fewer parameters compared with LSTM network. ConvLSTM equations can be written as follows, where “ $*$ ” denotes the convolution operator:

$$C_t = f_t \circ c_{t-1} + i_t \circ \tanh(W_{xc} * x_t + W_{hc}H_{t-1} + \mathbf{b}_c), \quad (6)$$

$$i_t = \sigma(W_{xi}x_t + W_{hi}h_{t-1} + W_{ci}c_{t-1} + \mathbf{b}_i), \quad (7)$$

$$f_t = \sigma(W_{xf}x_t + W_{hf}h_{t-1} + W_{cf}c_{t-1} + \mathbf{b}_f), \quad (8)$$

$$o_t = \sigma(W_{xo}x_t + W_{ho}H_{t-1} + W_{co} \circ c_t + \mathbf{b}_o), \quad (9)$$

$$H_t = o_t \circ \tanh(c_t). \quad (10)$$

## 2.2 ConvLSTMP3

In this study, an improved version of ConvLSTM, named ConvLSTMP3, is developed by parallelizing ConvLSTM model with three sub-network structures. Figure 2a shows the general topological structure of ConvLSTMP3, in which the leftmost,

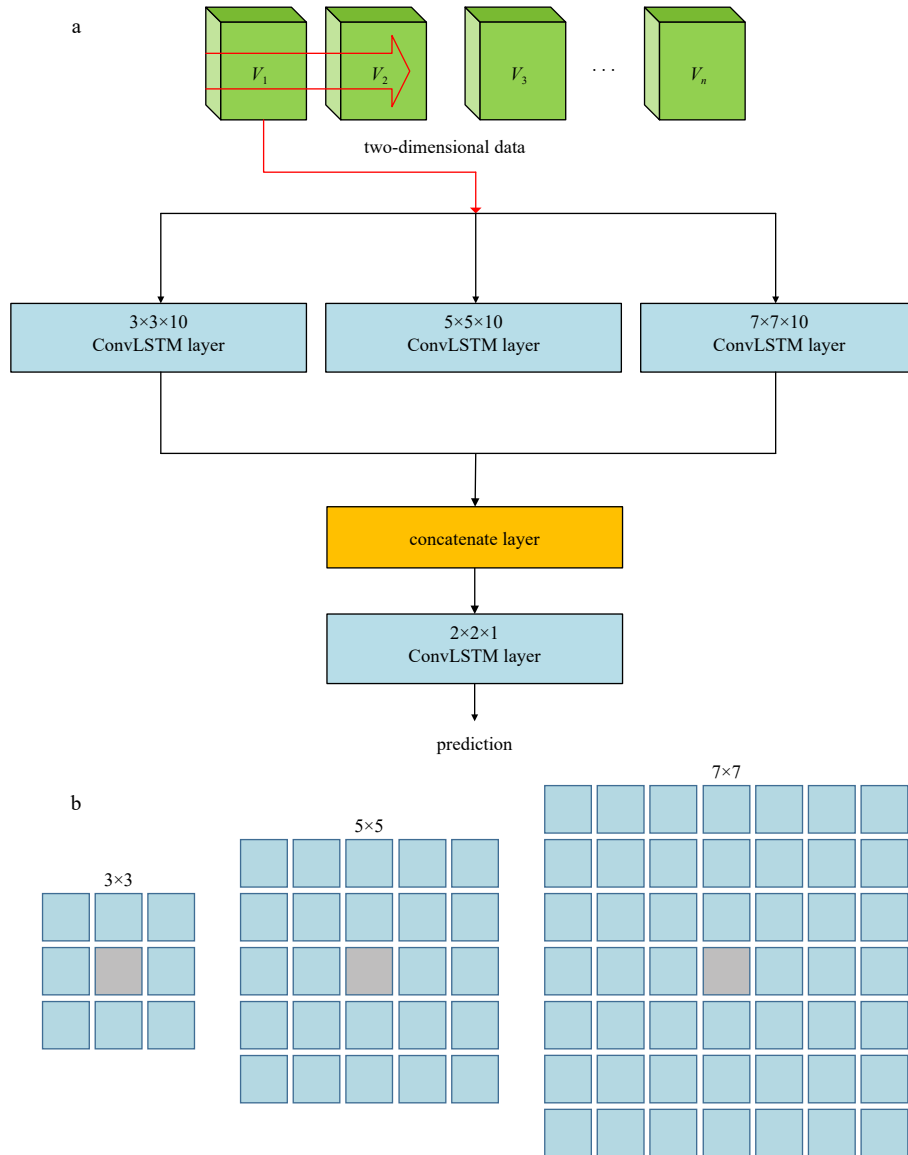


**Fig. 2.** The topologic structure of ConvLSTMP3 (a) and the adjacent grids (blue) of a target grid (gray) corresponding to the convolution kernels of size  $3 \times 3$ ,  $5 \times 5$ , and  $7 \times 7$  (b).  $V_i$  ( $i=1, 2, \dots, n$ ) represents datasets that are used to make the  $i$ -th-d SSH prediction for a target grid.

middle and rightmost sub-networks with 10 convolution kernels of size  $3\times 3$ ,  $5\times 5$ , and  $7\times 7$  aim to take the spatial information of the target grid as well as its 8, 24, and 48 adjacent grids (Fig. 2b), respectively. Here the grid is referred to the geographical cell that is formed by the intersection of latitude and longitude. Each sub-network can output 10 feature maps and the information from three subnetworks can be combined from the concatenate layer to produce 30 feature maps. The final  $2\times 2\times 1$  ConvLSTM reduces 30 feature maps of the concatenate layer to one feature map.

**2.3 ConvLSTM models for comparison**

We design extra four ConvLSTM models for comparison with our ConvLSTMP3, denoted as ConvLSTMS1, ConvLSTMP1, ConvLSTMP2 and ConvLSTMS4, respectively, as shown in Figs 3a–d. ConvLSTM is a classical LSTM model with two stacks, which only considers the temporal relationship of data without considering the spatial relationship. With only one path designed, ConvLSTMP1 considers the spatial-temporal relationship of 9 adjacent grids of each grid, while with two sub-networks, ConvLSTMP2 consider both the spatial-temporal relationship between 9 and 25

adjacent grids of each grid. ConvLSTMS4 has the same convolution kernels as ConvLSTMP3 except that the convolution kernels are serially connected.

**2.4 15-d consecutive prediction**

The 15-d consecutive prediction is made by adopting the predicted values as historical values for the input of ConvLSTMP3, as shown in Fig. 4. For a certain grid and a 15-d prediction cycle, the prediction begins with the use of historical SSHs of the last 15 d (i.e.,  $D_0-N+1, D_0-N+2, \dots, D_0$ , here  $N=15$  and  $D_0$  denotes the current day) as the input of ConvLSTMP3 to predict the SSHs on the next day ( $D_0+1$ ). After that, the historical SSHs of the last 14 d (i.e.,  $D_0-N+2, \dots, D_0$ , here  $N=15$ ) and the predicted SSHs on the day ( $D_0+1$ ) are taken as input of ConvLSTMP3 to predict the SSHs on the day ( $D_0+2$ ). By repeating this procedure, we can obtain the 15-d SSH prediction on each grid from day ( $D_0+1$ ) to day ( $D_0+15$ ). After the 15-d prediction cycle is done, we move to the next prediction cycle by taking ( $D_0+1$ ) as the current day; as such, we finally obtain the consecutive 15-d SSH prediction for a period from 6 January 2011 to 31 December 2012.

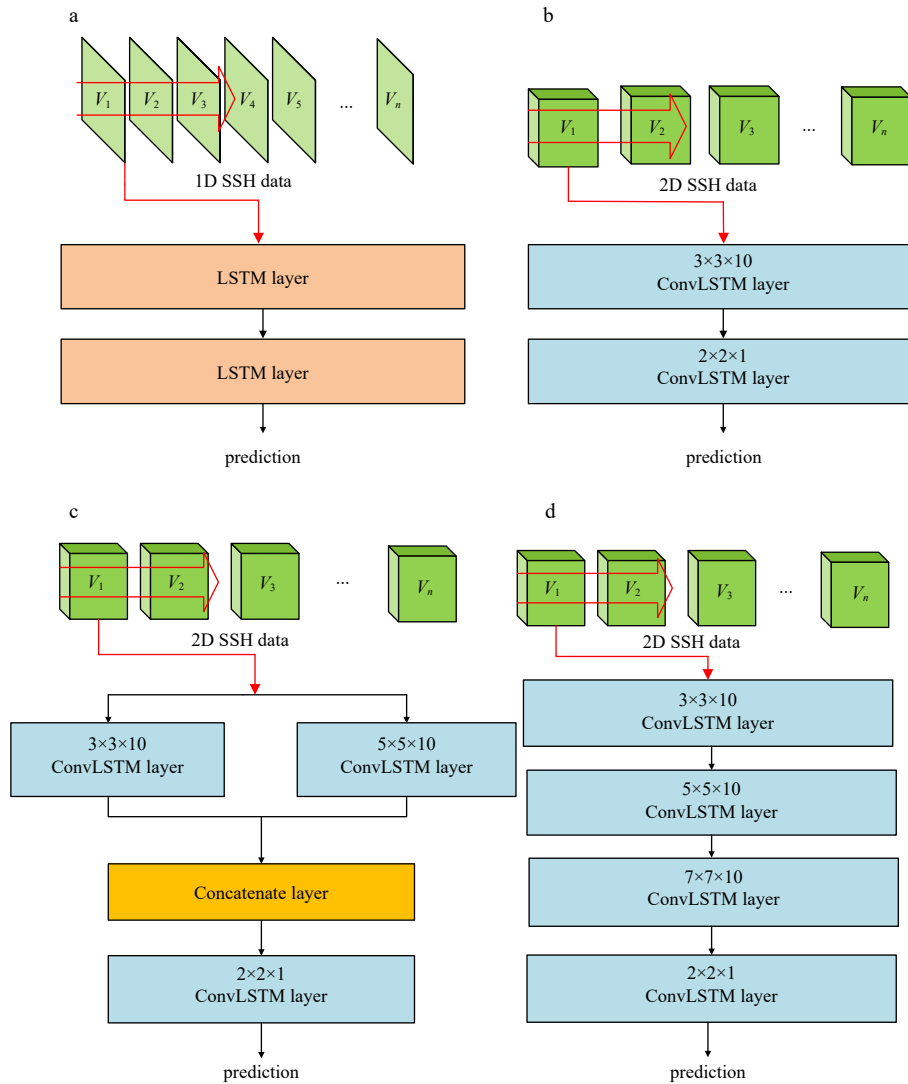


**Fig. 3.** The topologic structures of four models: LSTMS1 (a), ConvLSTMP1 (b), ConvLSTMP2 (c) and ConvLSTMS4 (d).  $V_i$  ( $i=1, 2, \dots, n$ ) represents datasets that are used to make the  $i$ -th-d SSH prediction for a target grid. 1D here means only a time series of SSH data on the target grid, while 2D means multiple time series of SSH data on the target grid as well as its adjacent grids.

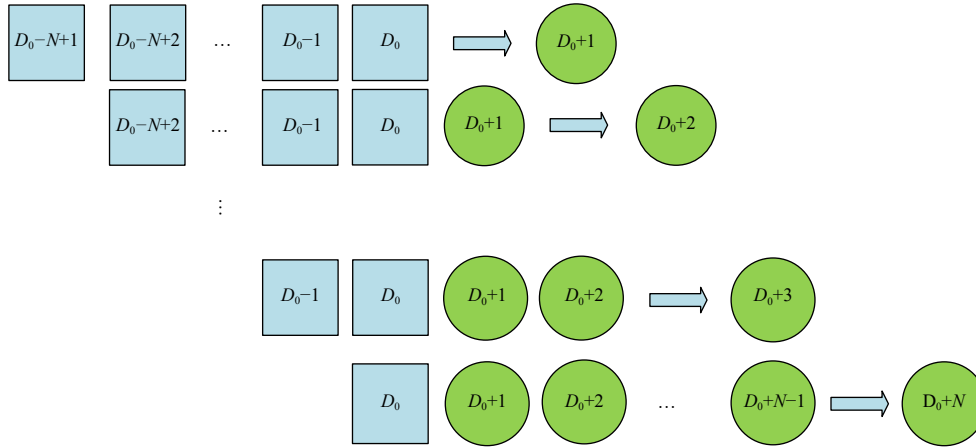


**Fig. 4.** A schematic diagram illustrating a 15-d prediction cycle. The squares and circles represent the historical SSHs and predicted SSHs, respectively. The squares or circles behind the arrows represent the input of ConvLSTMP3 and the circles ahead the arrows represent the output (prediction).  $D_0$  denotes the current day of the prediction cycle, and  $N$  is the length of prediction cycle which is set to 15 (days).

### 2.5 Experimental design

A  $5.5^\circ \times 5.5^\circ$  region ( $10.0^\circ$ – $15.5^\circ$ N,  $109.6^\circ$ – $115.1^\circ$ E, denoted by A) of the SCS located east off Vietnam, is chosen for the deep learning experiments for SSH prediction, as shown in Fig. 5. This region is featured with mesoscale eddies and offshore currents driven by summer monsoon. The daily SSHs in the selected region from the reanalysis dataset of South China Sea (REDOS) (Zeng et al., 2014) from 1 January 1992 to 31 December 2011 with a resolution of  $(1/10)^\circ \times (1/10)^\circ$  is used for the deep learning, which counts to a sample number of 7 305 (days) in time. With the same resolution as REDOS, the selected region A has a total grid number of  $55 \times 56 = 3\,080$ . Since the baseline of the deep-learning-based SSH prediction method is to deal with the SSH prediction problem as the spatial-temporal series prediction problem, we treat the SSH data of Region A as 7 305 two-dimensional ( $55 \times 56$ ) matrices or images arranged in temporal order. The SSH data of about 80% days from 1 January 1992 to 1 January 2008 are used to train ConvLSTMP3, 10% days from 2 January 2008 to 1 January 2010 are used for evaluation, and the remaining data of about 10% days from 2 January 2010 to 31 December 2011 are used for testing. In the training process, ConvLSTMP3 is trained by inputting the historical or predicted SSHs of the 15 d to predict the SSHs of the next 15 d. The input data length of 15 d for training ConvLSTMP3, which is the only parameter that LSTM needs to set, is chosen after a set of experiments with different input data lengths, considering the accuracy, efficiency and computation resources. The optimization algorithm of the ConvLSTMP3 employs the Adam algorithm, with the size of each mini-batch being 200. The Adam algorithm is an optimization algorithm commonly used in deep learning, which is able to make the neural network adjust the parameters to the global optimal solution fast. The learning rate is set to 0.001 to control the update ratio of the model. All the experiments are performed on a PC with an I7-8750H processor and 32 GB memory.

### 3 Results

The root mean squared error (RMSE) and prediction accuracy (ACC) are used to evaluate the prediction skill of different models, which are defined as follows:

$$\text{RMSE} = \sqrt{\frac{\sum_{i=1}^n (h_i^p - h_i^t)^2}{n}}, \quad (11)$$

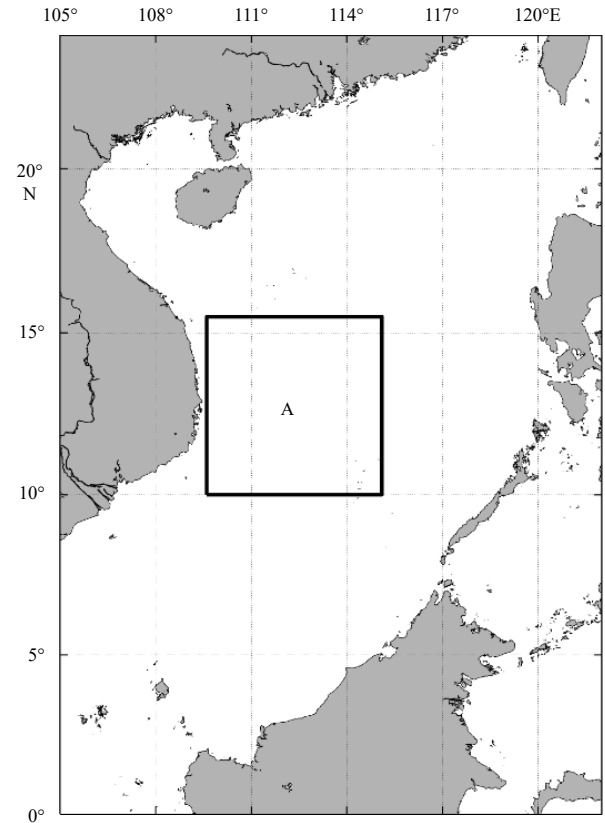


**Fig. 5.** The  $5.5^\circ \times 5.5^\circ$  region (denoted by A) of the SCS for the deep learning experiments for SSH prediction.

$$\text{ACC} = 1 - \frac{1}{n} \sum_{i=1}^n \frac{|h_i^p - h_i^t|}{h_i^t}, \quad (12)$$

where  $h_i^p$  and  $h_i^t$  are the predicted and ground truth values at  $i$ -th grid point, respectively, and  $n$  is the total number of grid points.

Figure 6 shows the RMSE and ACC of the consecutive 15-d prediction averaged over the testing period from 6 January 2010 to 31 December 2011 from different schemes for Region A. It is

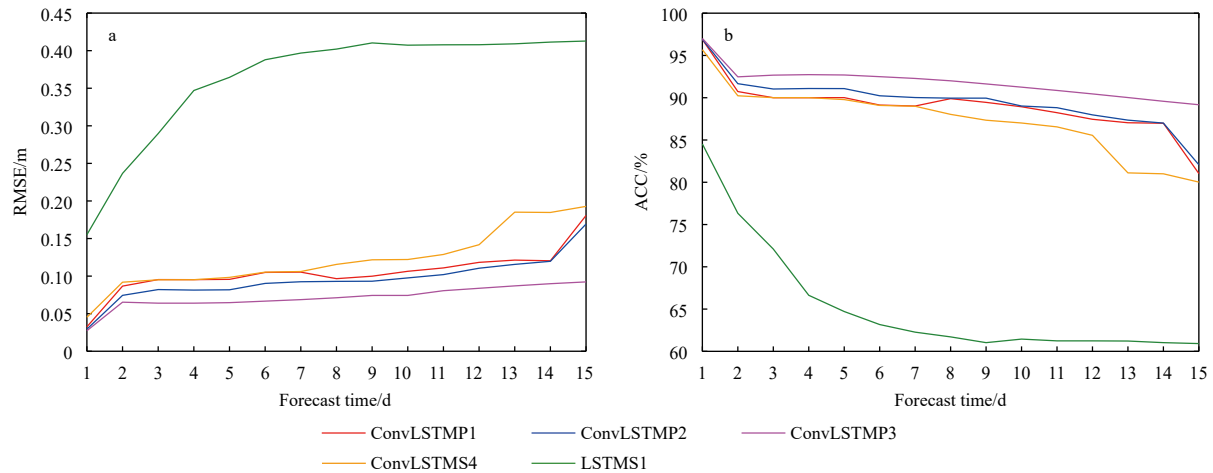


**Fig. 6.** The RMSE and ACC of the 15-d consecutive prediction averaged over the testing period from 6 January 2010 to 31 December 2011 from different schemes.

obvious that ConvLSTMP3 gives the best performance of the 15-d SSH prediction in comparison with other schemes, with a mean RMSE of 0.057 m and ACC of 93.4% averaged over the 15-d prediction period.

As an example, we select a summertime period of 1–15 August 2011 to see the performance of ConvLSTMP3 in the prediction of mesoscale eddies and offshore currents in Region A by a comparison with a state-of-the-art dynamical ocean model, i.e., the regional ocean model system (ROMS). ROMS is based on the Navier-Stokes equations and was used to generate the ground truth dataset REDOS by assimilating various observations. To compare the prediction skill of ConvLSTMP3 with that of ROMS, we run ROMS without data assimilation for 15 d starting on 1 August 2011. To be fair, the prediction by ROMS uses the same initial conditions from REDOS as those for ConvLSTMP3 and the same model configuration as those for producing REDOS (Zeng et al., 2015) which covers the entire SCS, while the lateral boundary conditions and the surface forcings (including winds, sensible heat fluxes and latent heat fluxes) are from the same data sources as those for producing REDOS but are climatological mean of August. Figure 7 presents the SSHs from the ground truth and the predictions by ConvLSTMP3 and ROMS, superimposed by the SSH-derived geostrophic currents. The ground truth SSHs show that there is an anticyclonic eddy in the east of Region A which weakened and diminished gradually, whereas a cyclonic eddy developed and intensified in the west of Region A. ConvLSTMP3 well predicts the location and temporal evolution of the two eddies, but slightly underestimates their intensity; ROMS seems to well predict the location and intensity of the two eddies but is not able to predict their temporal evolution. Besides the eddy-related SSHs, ConvLSTMP3 also well predicts the SSH pattern associated with the northeastward offshore currents east off Vietnam coast, but with weaker SSH gradient compared to that from the ground truth and ROMS, which leads to weaker offshore currents. Table 1 gives the RMSE and ACC of the SSH predictions by ConvLSTMP3 and ROMS for the period of 1–15 August 2011. The 15-d-mean RMSE (ACC) of the SSH prediction by ConvLSTMP3 is 0.057 m (93.4%), while that by ROMS is 0.072 m (89.7%), suggesting that ConvLSTMP3 achieves an encouraging prediction skill which is comparable to or even slightly better than that of ROMS. It is worthwhile noting that the computa-

tion resource needed for ConvLSTMP3 to make the 15-d prediction is about 100 times less than that for ROMS (Table 2, the CPU cores used for ConvLSTMP3 and ROMS are 1 and 112, respectively), although considerable time (about 32-h CPU time) is needed for the training of ConvLSTMP3 which is similar to the process of building up a full-dynamics ocean model. Therefore, ConvLSTMP3 has great advantage in terms of fast prediction for emergency requirement given that the training is done in advance.

Besides the comparison with ROMS, it is also interesting to compare the performance of ConvLSTM with that of CNN, LSTM and gated recurrent unit (GRU). While LSTM has three gates, GRU has only two gates with fewer parameters and thus requires less computing resource. Considering that the data of spatio-temporal series are three-dimensional, 3D CNN is used for the comparison. As shown in Table 3, LSTM and GRU have similar ACC scores in the SSH prediction that are much lower than those of ConvLSTM or CNN, probably due to the fact that both LSTM and GRU consider only one-dimensional time series data in either training or prediction; the performance of 3D CNN is comparable to that of ConvLSTM, but ConvLSTM has slightly higher ACC scores. Given that 3D CNN requires much more computing resources than ConvLSTM, we conclude that ConvLSTM performs the best among these algorithms in the SSH prediction.

#### 4 Conclusions

A SSH prediction model, called ConvLSTMP3, is developed based on deep learning techniques. The ConvLSTMP3 model can extract spatial information of non-image two-dimensional SSHs by convolution operation and make use of SSH correlation in different spatial extents through three parallel sub-network. The application of ConvLSTMP3 in a region of the SCS using a reanalysis dataset for training and testing indicates that ConvLSTMP3 has a promising skill in the SSH prediction with a 15-d-mean RMSE of 0.057 m and ACC of 93.4% averaged over the testing period of about two years, and it outperforms other deep-learning-based models, including LSTM, GRU and CNN. In particular, ConvLSTMP3 well predicts the spatial patterns and temporal evolution of mesoscale eddies as well as offshore currents in the region of the SCS, and its prediction skill is at least comparable to that of the full-dynamics ocean model ROMS which needs huge amount of computation for the prediction (about 100 times larger than that

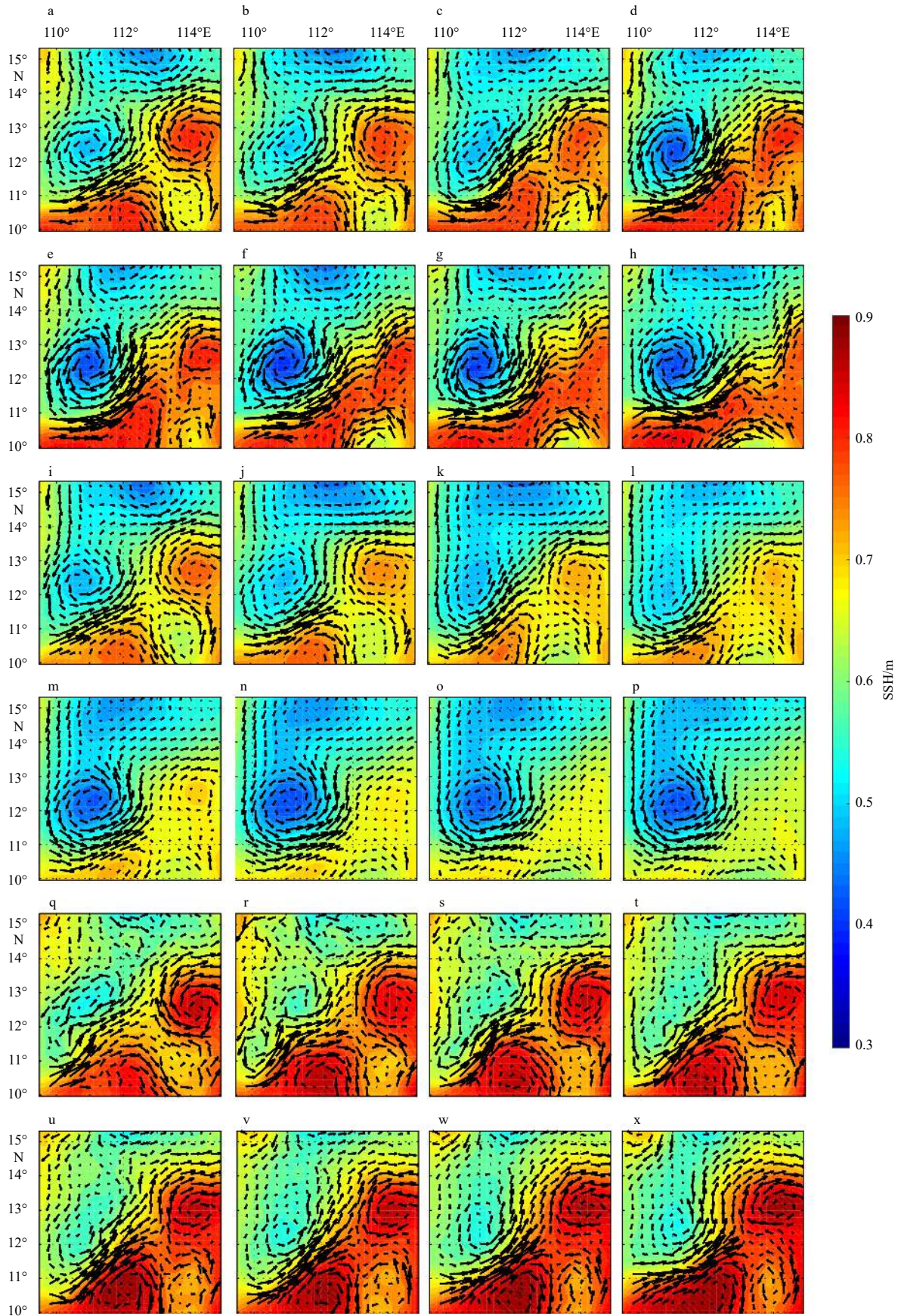


**Fig. 7.** The ground truth (a-h) and the predicted SSHs by ConvLSTMP3 (i-p) and ROMS (q-x) obtained from August 1 to 15, 2011 in every other day. The black arrows represent the SSH-derived geostrophic currents.

**Table 1.** The RMSE and ACC of the SSH predictions by ConvLSTMP3 and ROMS during the period of 1–15 August 2011

Period	Item			
	RMSE/m		ACC/%	
	ConvLSTMP3	ROMS	ConvLSTMP3	ROMS
Day 1	0.028	0.048	96.4	93.4
Day 2	0.017	0.073	98.0	88.6
Day 3	0.027	0.069	96.2	89.5
Day 4	0.033	0.064	96.3	90.2
Day 5	0.039	0.069	95.0	89.5
Day 6	0.051	0.055	93.0	92.3
Day 7	0.049	0.064	93.9	91.1
Day 8	0.049	0.067	93.8	90.4
Day 9	0.067	0.069	91.6	90.4
Day 10	0.055	0.079	93.5	88.4
Day 11	0.066	0.082	92.2	87.7
Day 12	0.083	0.073	89.4	89.8
Day 13	0.076	0.078	90.3	89.0
Day 14	0.085	0.076	89.5	89.6
Day 15	0.077	0.099	91.3	86.0
15-d mean	0.057	0.072	93.4	89.7

**Table 2.** The configurations of the hardware and software as well as the corresponding CPU time used for the 15-d prediction by ConvLSTMP3 and ROMS

	Hardware configuration	Software configuration	CPU time/s
ConvLSTMP3	Intel (R) Core (TM) i7-8750H (2.2 GHz) processor, 32 GB memory (total number used: 1)	Python 3.6.0	3.695
ROMS	Intel (R) Xeon (R) Gold 6 132 (2.60 GHz) processor, 125 GB memory (total number used: 112)	Mvapich2 2.2b	5.451

**Table 3.** The ACC of the SSH predictions by LSTM, GRU, CNN and ConvLSTMP3 during the period of 1–15 August 2011

Periods	Item			
	ACC/% (LSTM)	ACC/% (GRU)	ACC/% (3D CNN)	ACC/% (ConvLSTM)
Day 1	84.53	84.77	94.8	96.4
Day 2	76.33	77.33	95.0	98.0
Day 3	72.10	72.20	94.2	96.2
Day 4	66.63	66.67	95.3	96.3
Day 5	64.71	64.71	94.0	95.0
Day 6	63.17	63.23	93.0	93.0
Day 7	62.27	63.01	93.0	93.9
Day 8	61.71	62.00	92.8	93.8
Day 9	61.03	61.07	90.6	91.6
Day 10	61.45	61.55	91.5	93.5
Day 11	61.24	61.43	92.0	92.2
Day 12	61.24	61.24	89.0	89.4
Day 13	61.22	61.21	89.0	90.3
Day 14	61.03	61.05	89.1	89.5
Day 15	60.92	61.00	88.6	91.3
15-d mean	65.30	65.50	92.1	93.4

needed for ConvLSTMP3). Therefore, our study suggests that the deep learning techniques, here referred to as ConvLSTMP3, are very useful and effective in the SSH prediction, and could be an alternative way in the operational prediction of ocean environments in the future, particularly desirable for the emergency needs.

## References

- Braakmann-Folgmann A, Roscher R, Wenzel S, et al. 2017. Sea level anomaly prediction using recurrent neural networks. arXiv preprint arXiv: 1710.07099
- Cho K, Van Merriënboer B, Gulcehre C, et al. 2014. Learning phrase representations using RNN encoder-decoder for statistical machine translation. arXiv preprint arXiv: 1406.1078v1, 1724–1734
- De Bézenac E, Pajot A, Gallinari P. 2019. Deep learning for physical processes: Incorporating prior scientific knowledge. *Journal of Statistical Mechanics: Theory and Experiment*, 2019(12): 124009, doi: [10.1088/1742-5468/ab3195](https://doi.org/10.1088/1742-5468/ab3195)
- Hochreiter S, Schmidhuber J. 1997. Long short-term memory. *Neural Computation*, 9(8): 1735–1780, doi: [10.1162/neco.1997.9.8.1735](https://doi.org/10.1162/neco.1997.9.8.1735)
- Huang X J, Shan J J, Vaidya V. 2017. Lung nodule detection in CT using 3d convolutional neural networks. In: 2017 IEEE 14th International Symposium on Biomedical Imaging. Melbourne, VIC,

- Australia: IEEE, 379–383
- Iudicone D, Santoleri R, Marullo S, et al. 1998. Sea level variability and surface eddy statistics in the Mediterranean Sea from TOPEX/POSEIDON data. *Journal of Geophysical Research: Oceans*, 103(C2): 2995–3011, doi: [10.1029/97JC01577](https://doi.org/10.1029/97JC01577)
- Jacobs G A, Hogan P J, Whitmer K R. 1999. Effects of eddy variability on the circulation of the Japan/East Sea. *Journal of Oceanography*, 55(2): 247–256, doi: [10.1023/A:1007898131004](https://doi.org/10.1023/A:1007898131004)
- Ji Shuiwang, Xu Wei, Yang Ming, et al. 2013. 3D Convolutional neural networks for human action recognition. *IEEE Transactions on Pattern Analysis and Machine Intelligence*, 35(1): 221–231, doi: [10.1109/TPAMI.2012.59](https://doi.org/10.1109/TPAMI.2012.59)
- Kumar N K, Savitha R, Al Mamun A. 2017. Regional ocean wave height prediction using sequential learning neural networks. *Ocean Engineering*, 129: 605–612, doi: [10.1016/j.oceaneng.2016.10.033](https://doi.org/10.1016/j.oceaneng.2016.10.033)
- Ma Xiaolei, Tao Zhimin, Wang Yinhai, et al. 2015. Long short-term memory neural network for traffic speed prediction using remote microwave sensor data. *Transportation Research Part C: Emerging Technologies*, 54: 187–197, doi: [10.1016/j.trc.2015.03.014](https://doi.org/10.1016/j.trc.2015.03.014)
- Mason E, Pascual A, McWilliams J C. 2014. A new sea surface height-based code for oceanic mesoscale eddy tracking. *Journal of Atmospheric and Oceanic Technology*, 31(5): 1181–1188, doi: [10.1175/JTECH-D-14-00019.1](https://doi.org/10.1175/JTECH-D-14-00019.1)
- McWilliams J C. 1985. Submesoscale, coherent vortices in the ocean. *Reviews of Geophysics*, 23(2): 165–182, doi: [10.1029/RG023i002p00165](https://doi.org/10.1029/RG023i002p00165)
- Morrow R, Coleman R, Church J, et al. 1994. Surface eddy momentum flux and velocity variances in the Southern Ocean from Geosat altimetry. *Journal of Physical Oceanography*, 24(10): 2050–2071, doi: [10.1175/1520-0485\(1994\)024<2050:SEMFAV>2.0.CO;2](https://doi.org/10.1175/1520-0485(1994)024<2050:SEMFAV>2.0.CO;2)
- Reckinger S, Fox-Kemper B, Bachman S, et al. 2014. Anisotropic mesoscale eddy transport in ocean general circulation models. In: 67th Annual Meeting of the Aps Division of Fluid Dynamics. San Francisco, California: Bulletin of the American Physical Society, 59(20): 23–25
- Seki M P, Bidigare R R, Lumpkin R, et al. 2001. Mesoscale cyclonic eddies and pelagic fisheries in Hawaiian waters. In: MTS/IEEE Oceans 2001. An Ocean Odyssey. Conference Proceedings. Honolulu, HI, USA: IEEE
- Shi Xinglian, Chen Zhourong, Wang Hao, et al. 2015. Convolutional LSTM network: A machine learning approach for precipitation nowcasting. In: Proceedings of the 28th International Conference on Neural Information Processing Systems. Cambridge, MA, USA: MIT Press, 802–810
- Shin H C, Roth H R, Gao Mingchen, et al. 2016. Deep convolutional neural networks for computer-aided detection: CNN architectures, dataset characteristics and transfer learning. *IEEE Transactions on Medical Imaging*, 35(5): 1285–1298, doi: [10.1109/TMI.2016.2528162](https://doi.org/10.1109/TMI.2016.2528162)
- Song Tao, Wang Ziheng, Xie Pengfei, et al. 2020. A novel dual path gated recurrent unit model for sea surface salinity prediction. *Journal of Atmospheric and Oceanic Technology*, 37(2): 317–325, doi: [10.1175/JTECH-D-19-0168.1](https://doi.org/10.1175/JTECH-D-19-0168.1)
- Soong Y S, Hu J H, Ho C R, et al. 1995. Cold-core eddy detected in South China Sea. *Eos, Transactions American Geophysical Union*, 76(35): 345–347
- Szegedy C, Vanhoucke V, Ioffe S, et al. 2016. Rethinking the Inception Architecture for Computer Vision. Las Vegas, NV, USA: IEEE, 2818–2826
- Szegedy C, Liu Wei, Jia Yangqing, et al. 2015. Going deeper with convolutions. *Proceedings of the IEEE Conference on Computer Vision and Pattern Recognition*. Boston, MA, USA: IEEE, 1–9
- Wang Liping, Koblinsky C J, Howden S. 2000. Mesoscale variability in the South China Sea from the TOPEX/Poseidon altimetry data. *Deep Sea Research Part I: Oceanographic Research Papers*, 47(4): 681–708, doi: [10.1016/S0967-0637\(99\)00068-0](https://doi.org/10.1016/S0967-0637(99)00068-0)
- Weiss J B, Grooms I. 2017. Assimilation of ocean sea-surface height observations of mesoscale eddies. *Chaos*, 27(12): 126803, doi: [10.1063/1.4986088](https://doi.org/10.1063/1.4986088)
- Yang Fengyu, Feng Tao, Xu Ganyang, et al. 2020. Applied method for water-body segmentation based on mask R-CNN. *Journal of Applied Remote Sensing*, 14(1): 014502
- Zeng Xiangming, Li Yizhen, He Ruoying. 2015. Predictability of the loop current variation and eddy shedding process in the Gulf of Mexico using an artificial neural network approach. *Journal of Atmospheric and Oceanic Technology*, 32(5): 1098–1111, doi: [10.1175/JTECH-D-14-00176.1](https://doi.org/10.1175/JTECH-D-14-00176.1)
- Zeng Xuezhi, Peng Shiqiu, Li Zhijin, et al. 2014. A reanalysis dataset of the South China Sea. *Scientific Data*, 1: 140052, doi: [10.1038/sdata.2014.52](https://doi.org/10.1038/sdata.2014.52)
- Zhang Qin, Wang Hui, Dong Junyu, et al. 2017. Prediction of sea surface temperature using long short-term memory. *IEEE Geoscience and Remote Sensing Letters*, 14(10): 1745–1749, doi: [10.1109/LGRS.2017.2733548](https://doi.org/10.1109/LGRS.2017.2733548)
- Zhang Zhengguang, Wang Wei, Qiu Bo. 2014a. Oceanic mass transport by mesoscale eddies. *Science*, 34(6194): 322–324
- Zhang Chunhua, Xi Xiaoliang, Liu Songtao, et al. 2014b. A mesoscale eddy detection method of specific intensity and scale from SSH image in the South China Sea and the Northwest Pacific. *Science China Earth Sciences*, 57(8): 1897–1906, doi: [10.1007/s11430-014-4839-y](https://doi.org/10.1007/s11430-014-4839-y)
- Zhang Yuanyuan, Zhao Dong, Sun Jiande, et al. 2016. Adaptive convolutional neural network and its application in face recognition. *Neural Processing Letters*, 43(2): 389–399, doi: [10.1007/s11063-015-9420-y](https://doi.org/10.1007/s11063-015-9420-y)